Developments in the Built Environment 12 (2022) 100098

Contents lists available at ScienceDirect

Developments in the Built Environment

journal homepage: www.sciencedirect.com/journal/developments-in-the-built-environment

Improvement of treated spent pot lining reactivity in cementitious material by calcination

Victor Brial [a], Hang Tran [b], Luca Sorelli [b], David Conciatori [b], Claudiane M. Ouellet-Plamondon [a,*]

[a] Department of Construction Engineering, École de technologie supérieure, Université du Québec, Canada
[b] Department of Civil and Water Engineering, Université Laval, Canada

ARTICLE INFO

Keywords:
Low caustic leaching liming
Treated spent pot lining
Blended cement
Hazardous waste
Aluminum
Supplementary cementitious materials

ABSTRACT

Treating spent pot lining by the Low Caustic Leaching and Liming (LCLL) process creates an inert non-hazardous residue called LCLL Ash. Ground as a fine powder and calcined, LCLL Ash showed a pozzolanic behavior in cement. The effect of the calcination temperatures on LCLL Ash reactivity was studied by compressive strength activity index, Frattini tests, and RILEM R^3 tests, followed by XRD analysis. When calcinating LCLL Ash at temperatures below 800 °C, no differences in reactivity were seen between calcined and non-calcined LCLL Ash. At 800 °C, the formation of nepheline caused an alkalis uptake, showing a slightly lower reactivity of LCLL Ash than cement at 112 days. Beyond 800 °C up to 1200 °C, calcined LCLL Ash manifested better amorphization of phases and increased reactivity, similar to cement at 112 days. Finally, neither delay on hydration nor hydro-reactivity was observed with calcined LCLL Ash starting at 800 °C.

1. Introduction

Reducing greenhouse gas emissions to limit the effects of global warming is one of the greatest challenges of the 21st century. The production of cement for the construction industry is one of the main sources of anthropogenic CO_2 emissions, which represents 5–8% of annual global CO_2 emissions (Friedlingstein et al., 2020; Lehne and Preston, 2018). Numerous optimizations have been carried out on cement production processes to reduce the energy consumption of cement factories and to make them less polluting. These efforts have led to a decrease of about 42% in energy consumption between 1950 and 2000 (Van Oss and Padovani, 2003). However, around 750 kg–950 kg of CO_2 is emitted to produce 1 ton of Portland clinker, with 60% due to unavoidable decarbonation reactions (Strazza et al., 2011; Hewlett and Liska, 2019; WBCSD, 2016). The use of supplementary cementitious materials (SCM) to reduce the amount of cement in concrete and the overall environmental impact is currently one of the preferred solutions (Kajaste and Hurme, 2016; Shanks et al., 2019; WBCSD, 2009). Most conventional SCMs are usually comprised of industrial byproducts or wastes, such as fly ash or blast furnace slags (Hewlett and Liska, 2019; Tokyay, 2016). Besides decreasing the carbon footprint of concrete, SCMs can also improve its properties, allow a better use of non-conventional wastes and reduce landfill content (Agrawal et al., 2004). However, the increasing use of renewable energy has led to a decrease in the availability of certain SCMs such as coal fly ash. Therefore, to produce environmentally friendly concrete, new sources of SCMs compatible with cement must be found.

Spent pot lining (SPL) is a hazardous industrial waste issued from the primary aluminum industry, and generated by the aluminum electrolytic tanks lining consisting of carbon and refractory bricks. Each ton of primary aluminum generates about 22 kg of SPL (Birry et al., 2016), which represents a volume of 70,000 tons of SPL in Canada annually. These quantities remain important from a local perspective for regions associated to the treatment of SPL due to its hazardous nature. SPL is considered hazardous as contact with water may lead to the generation of explosive gases according to Eqs. (1)–(3) (Øye, 2017; Al Jawi et al., 2020; Broek and Øye, 2018) and the leaching of cyanide and fluoride (Øye, 2017; Broek and Øye, 2018; Kimmerle et al., 1993). The reaction of SPL and water is called hydroreactivity. Prior to treatment, SPL is separated into two parts: the cathode providing a carbon-rich material and the electrolytic tanks containing refractory materials. This separation step optimizes the valorization process by creating rich carbonaceous materials that can be used as fuel and mineral materials that would generally be landfilled after treatment.

* Corresponding author. École de technologie supérieure, Université du Québec, 1100 rue Notre-Dame Ouest, Montréal, Québec, H3C 1K3, Canada.
E-mail address: claudiane.ouellet-plamondon@etsmtl.ca (C.M. Ouellet-Plamondon).

https://doi.org/10.1016/j.dibe.2022.100098
Received 7 October 2022; Received in revised form 6 November 2022; Accepted 10 November 2022
Available online 15 November 2022

$$2\,Al + 2\,NaOH + 2\,H_2O = 3\,H_2 + 2\,NaAlO_2 \quad (1)$$

$$Al_4C_3 + 6\,H_2O = 3\,CH_4 + 2\,Al_2O_3 \quad (2)$$

$$AlN + 3\,H_2O = NH_3 + Al(OH)_3 \quad (3)$$

Different ways of recovering SPL in the cement industry have been studied in order to avoid burying. Using the SPL as a raw material without pretreatment despite its hazardous character is common in cement plants in Europe, Asia, Middle East, and Brazil (Al Jawi et al., 2020; Broek and Øye, 2018; Nunez, 2020; Personnet, 1999). One advantage to the addition of SPL in the raw meal that has been observed is a drop of 20–100 °C from the initial clinkerization temperature following an increase in the fluoride content in the raw meal. Additionally, a linear relationship has been found between a temperature drop and an increase in the SPL replacement percentage. (Al Jawi et al., 2020; Gomes et al., 2005). This lower clinkerization temperature can decrease fossil fuel consumption and the CO_2 emissions respectively by 4% and 1%. The SPL addition percentage in the raw meal is, however, limited to between 0.2% and 0.75% to avoid durability issues caused by alkali-silica reactions attributed to the high sodium content of the SPL (Al Jawi et al., 2020; Broek and Øye, 2018; Nunez, 2020; Gomes et al., 2005). Moreover, due to SPL's high percentage of fluoride, this practice is currently not allowed in the North American cement industry.

Developed in the early 2000, in Quebec, a pyrometallurgical treatment of SPL generate a by-product called glass frit (Fares, 2008). This compound's reactivity was similar to that of a latent hydraulic binder, and it behaved similarly to slag (Fares, 2008; Laldji and Tagnit-Hamou, 2016). The mechanical properties of binary GF mixtures were similar to those of unblended mixes. Moreover, glass frit exhibited better durability performance against freezing thaw, chloride permeability, and against alkali-silica reaction (Laldji and Tagnit-Hamou, 2016; Nova Pb inc, 2004). The Low Caustic Leaching & Liming (LCL&L) process, developed by Rio Tinto in the early 1990s, treat SPL to generate an inert material through a hydrometallurgical process. The refractory rich second cut of SPL changes into a grey LCLL Ash powder (an inert material) after treatment by the LCL&L process (Birry and Leclerc, 2016). Currently, the SPL treatment plant in Jonquière (Quebec) is the only plant in the world using the LCL&L process. The resulting grey powder (LCLL Ash) from the LCL&L process is constituted by a majority of silica and aluminum oxides, with minor fractions of sodium, and iron oxides. The present article is the continuation of a more global project studying use of treated SPL by LCL&L process as cementitious materials. In the first part of the project, the use of LCLL Ash in cement was studied by Brial et al. (2021), who found that it behaved much like an alkaline filler thanks to its significant concentration of low-soluble phases such as nepheline or albite. Moreover, in some conditions, depending on the temperature, chemistry, and pH, LCLL Ash provokes hydro-reactivity, which generates gas. However, after an additional calcination at 1050 °C, LCLL Ash's reactivity in cement is significantly improved, and it turns into a pozzolanic material, which is similar to what is seen with fly ashes, but without hydro-reactivity. In addition, due to the high availability of reactive alumina in calcined LCLL Ash, new hydrated phases, such as carboaluminate phases, may precipitate.

Mineral materials are often calcined to enhance their reactivity, as is commonly the case on clay or shale, where that is done to create reactive SCMs (Ambroise et al., 1985; Mather, 1958; Murat, 1983). This process may seem counter-intuitive when developing CO_2 emission reduction initiatives, but it does effectively reduce the carbon impact of cement. As an example, a lower carbon footprint is achieved by blending conventional cements with calcined shale or calcined clay (Scrivener et al., 2018). The emission reductions are associated with the use of blending materials having a lower calcination temperature than clinker, as well as with an absence of calcite decarbonation (Scrivener et al., 2018; Miller et al., 2018).

This article aims to explore a potential approach to a circular economy between two industries known for their high environmental impacts. This process would favor the use of local wastes from the aluminum industry into the cement industry and create a more sustainable binder for concrete production. This article is part of the project on the valorization of treated SPL by LCL&L process. The goal of this article is to analyze and understand the effect of calcination temperatures on the reactivity of LCLL Ash in cement. Hence, the aim is to answer the following questions:

(i.) How does calcination improve LCLL Ash reactivity?
(ii.) What is the optimum calcination temperature of LCLL Ash?

To answer these questions, an evaluation of the effect of calcination temperature ranging from 600 °C to 1200 °C on LCLL Ash was performed. For each calcination temperature of LCLL Ash tested, the mineralogical composition was analyzed by quantitative XRD Rietveld analysis to determine the phase change throughout the calcination process. The reactivity of the calcined LCLL Ash at different temperatures was then studied using the same methodology as Brial et al. (2021) with mortar compressive strength Frattini, R^3 tests and quantitative Rietveld X-ray diffraction.

2. Materials and methods

2.1. Materials

For the present work, Rio Tinto provided LCLL Ash from their treatment plant in Jonquière, QC, Canada. An Portland cement (PC, type GU provided by Ciment Québec, St Basile, QC, Canada) was used to prepare samples for Frattini tests and mortar mixes. A quartz powder, named Q, made by grinding graded Ottawa sand was used as a reference sample. The sample was used as a reactivity comparator against the calcined LCLL Ash.

The oxide composition of cement used for the blended mixes, for the LCLL Ash and for the quartz powder was measured by X-ray fluorescence (XRF) in fused glass beads after a loss of ignition at 1000 °C for 30 min. The oxide compositions of Portland cement, LCLL Ash and quartz powder are shown in Table 1. About 37% and 36% of silica and alumina content were respectively found in the LCLL Ash sample, indicating a composition similar to that of a calcined clay. More specifically, about 8% of sodium oxide was found in LCLL Ash, showing a higher alkali content than conventional clay but lower than glass powder (Mejdi et al., 2019). X-ray powder diffraction (XRD) with Rietveld analysis was used to analyze the mineralogical composition of the materials. The amorphous content was determined with a zincite (ZnO) external standard. The quantitative composition from XRD analysis of the cement, the LCLL Ash and the quartz powder are presented in Table 2.

LCLL Ash is mainly consisting of crystalline phases such as albite, nepheline, corundum, quartz and anorthite with a content in amorphous phases about 6%. As previously studied by Brial et al. (2021), the high content of crystalline phases gives LCLL Ash an inert behavior in cement which explains the additional treatment by calcination to increase LCLL Ash reactivity. Moreover, XRD results showed that sodium is mainly incorporated as plagioclase with low solubility in aqueous phases such as albite.

2.2. Methods

2.2.1. Calcined LCLL ash preparation

Raw LCLL Ash was initially ground with a Fritsch Pulverisette 9 vibrating cup mill in 100 g batches for 2 min 30 s at a speed of 1000 rpm. The ground samples were calcined for 2 h in a Nabertherm N11/H high temperature furnace from 600 °C to 1200 °C with a step of 50 °C. Three 200 g samples of ground LCLL Ash were calcined in individual 300 mL alumina crucibles at each calcination temperature. The samples were removed from the furnace at high temperature and cooled by air

Table 1
Chemical composition of cement and SCMs.

Percentage in weight (wt%)												
Oxide	**SiO_2**	**Al_2O_3**	**Fe_2O_3**	**CaO**	**MgO**	**SO_3**	**K_2O**	**Na_2O**	**TiO_2**	**P_2O_5**	**V_2O_5**	**LOI**
PC	19.17	4.69	3.61	61.52	2.4	3.98	1.06	0.25	0.25	0.14	0.01	2.62
LCLL Ash	37.18	36.29	7.36	3.04	0.38	0.06	0.77	8.23	0.75	0.12	0.03	5.72
Quartz	91.4	4.94	1.72	0.55	0.04	0	0.1	1.09	0.1	0.01	0.01	0

Table 2
Major mineralogical compositions of PC, LCLL Ash and quartz powder.

Phase	PC	LCLL Ash	Quartz
C_3S	63.3	–	–
C_2S	8.5	–	–
C_3A	3.6	–	–
C_4AF	11.3	–	–
Quartz	0.1	10.3	98.4
Corundum	–	13.7	–
Albite	–	8.5	–
Nepheline	–	20.9	–
Anorthite	–	12.2	1.2
Graphite	–	7.2	–
Mullite	–	3.4	–
Hematite	–	2.3	–
Magnetite	–	4.3	–
Fluorite		1.7	
β-Alumina		7.2	
Calcite	2.4	–	–
Amorphous	–	5.9	–

quenching on a metallic plate until reaching room temperature. The calcined LCLL Ash obtained from the 3 crucibles were mixed together and ground with the same vibrating cup grinder at different grinding times until a d_{50} of around 10 ± 1.5 μm was obtained. The particle size distribution (PSD) of each calcined LCLL Ash mix was measured by laser diffraction granulometry using a Malvern Mastersizer 3000 and using isopropanol as dispersant. To obtain the grinding time, a first estimate was made arbitrarily at 60 s using LCLL ash calcined at 1200 °C. The particle size was checked by laser diffraction particle size analysis and the grinding adjusted by adding or subtracting 30 s. Then a new sample was ground with the new grind time and the new control. For samples with a grinding time less than 30 s, the grinding time was adjusted with an interval of 5 s. The particle size distributions and the grinding time are respectively presented in Fig. 1a and b.

2.2.2. Mortar

The same methods as Brial et al. (2021) were used to evaluate mortar compressive strength. The mortar mixes were prepared and tested respectively according to ASTM C305 (ASTM International, 2015) and ASTMC109 (ASTM International, 2016) standards with a water binder ratio of 0.485 and replacement of cement by 20% of tested materials. After 24 h, the samples were demolded and placed in a moisture room at 23 ± 2 °C with relative humidity level of not less than 95%. At 1, 7, 28 and 112 days, the samples were tested to evaluate the mixes' strength activity index. For more information about the protocol used, refer to Brial et al. (2021).

2.2.3. Frattini tests

Frattini tests allow quantifying the pozzolanic reactivity by measuring calcium reductions. The samples were prepared and analyzed with the same methods as Brial et al. (2021). For each material, 3 samples were prepared by mixing 100 mL of distilled water with 4 g of tested materials and 16 g of Portland cement. The samples were left in a sealed plastic bottle in an oven at 40 °C. After 8 days, the calcium and hydroxyl ions concentration were respectively analyzed by ICP-OES and titration after a preliminary filtration with a 0.2 μm syringe filter. The quantification of pozzolanic reactivity is based on the ratio between the distance of each sample data point to the lime solubility curve given by the European standard EN 196–5 (British Standard Euronorm, 2005). This lime solubility curve is dependent of the hydroxyl (OH^-) concentration and is given by the European standard for hydroxyl concentration between 35 and 90 mmol/L according to Eq. (4):

$$[Ca^{2+}] = \frac{350}{[OH^-] - 15} \quad (4)$$

2.2.4. R^3: heat released and portlandite consumption

The R^3 tests were initially developed to quantify in limestone cement the reactivity of calcined clay. However, due to their ability to quantify other types of reactivity as hydraulic reaction, these tests were extended to other SCMs. The specific of these tests is the R^3 which recreates adequately the chemical composition of a limestone cement without cement grains. This allows the study of the reactivity of the tested materials without interference from the cement phases. The composition of the R^3 paste is given by Li et al. and is made of 33.33 g of portlandite ($Ca(OH)_2$), 11.11 g of SCM, and 5.56 g calcite ($CaCO_3$) in a 60 mL solution

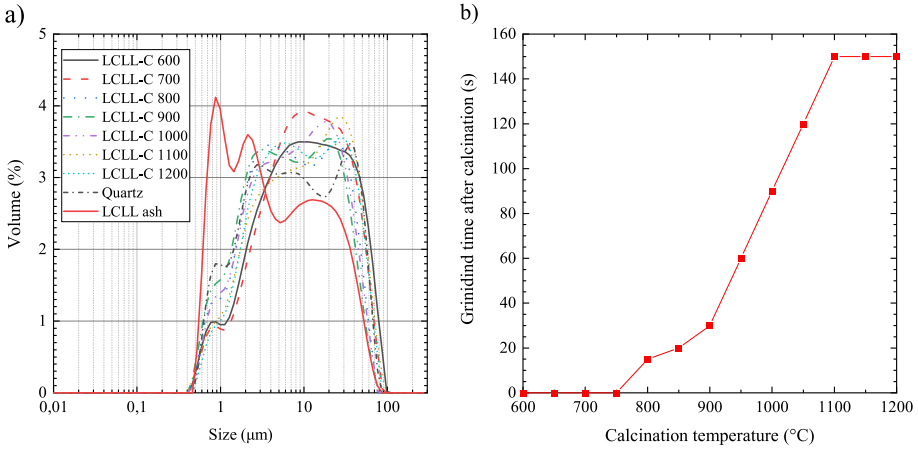

Fig. 1. a) Particle size analysis by laser granulometry; b) Secondary grinding time as a function of the calcination temperature.

of deionized water with 0.24 g of KSO_4 and 1.20 g KOH (Li et al., 2018). In the R^3 system, the reactivity was determined by measuring the portlandite consumption and the heat released at 7 days by isothermal calorimetry. Heat released was then plotted against the calcium hydroxide consumption and the type of reactivity of tested materials was determined according to the method described in (Suraneni et al., 2019). Isothermal calorimetry tests were carried out at 40 °C and each test had initial and final baselines recorded for 180 min. TGA analyses allowed measuring the portlandite consumption. To this end, samples retrieved from the R^3 calorimetry ampoules were first carefully rolled in adhesive tape to minimize glass contamination, and then broken to collect the paste. The hydration of the samples was stopped by solvent exchange as executed by (Snellings et al., 2018; Scrivener et al., 2016). Each TGA test was done on 50 mg of an anhydrous sample introduced in the crucible. Weight loss in the sample was recorded from 30 to 950 °C through a heating rate of 10 °C/min in a protective nitrogen atmosphere at a flow rate of 50 mL/min. The portlandite weight loss was determined by the tangent method described by (Scrivener et al., 2016), while the portlandite consumption was calculated as g/100 g SCM according to the method proposed by Li et al. (2018).

2.2.5. X-ray diffraction

To identify the phase phases which occurred during calcination, calcined LCLL Ash at different temperatures were analyzed by XRD. Moreover, to identify the new phases precipitated during the test R^3, the same samples used in the R^3 portlandite consumption test were also analyzed by quantitative XRD. For these tests, data were collected on a Bruker D8 Advance diffractometer operated at 40 kV and 40 mA using Cu K-alpha radiation. The R^3 paste samples were prepared by solvent exchange. The calcined LCLL Ash and hydrated R^3 paste sample analyzed by Rietveld analysis according to the same methods as Brial et al. (2021). In both cases, the amorphous content was determined with a zincite external standard corrected with the mass absorption coefficient. For more information about the parameters used to record XRD data, refer to Brial et al. (2021).

3. Results

3.1. Calcined LCLL Ash composition

Fig. 2a and b shows the composition of calcined LCLL Ash as a function of the calcination temperature measured by quantitative XRD analysis. The mineralogical composition was measured after cooling and grinding. Due to technical difficulties in observing and quantifying iron-rich phases by XRD, they were counted with the amorphous content.

In accordance with Wang et al. (2017), the main reactions at high temperature took place between the four main oxides, namely, SiO_2, Al_2O_3, Na_2O and CaO, according to the following equations:

$$Na_2O + Al_2O_3 + 6\ SiO_2 = 2\ NaAlSi_3O_8\ (\text{Albite}) \quad (5)$$

$$NaAlSi_3O_8 + Al_2O_3 + Na_2O = 3\ NaAlSiO_4\ (\text{Nepheline}) \quad (6)$$

$$Na_2O + CaAl_2Si_2O_8\ (\text{Anorthite}) = 2\ NaAlSiO_4 + CaO \quad (7)$$

$$NaAlSiO_4 + 2\ SiO_2 = NaAlSi_3O_8 \quad (8)$$

$$CaF_2 + Na_2O = 2\ NaF + CaO \quad (9)$$

From 600 °C to 800 °C, a slight increase in the formation of amorphous phases can be seen. However, changes in the mineralogical composition are also visible. Nepheline and anorthite concentrations increase by about 10% and 3.5% respectively. Conversely, a 4.5 and 3% decrease in the concentration of quartz and corundum, respectively, as well as the complete disappearance of mullite and fluorite are observed. According to Eq. (6), the formation of nepheline is attributable to the reaction between beta alumina, quartz and alumina. Similarly, the increase in anorthite is possibly attributed to the reaction of the mullite with calcium oxide (Li et al., 2012; Wu et al., 2009). This calcium oxide can only come from the transformation of fluorite into sodium fluoride (NaF) through the high presence of available sodium. From 850 °C to 1200 °C, a significant increase seen in the formation of amorphous phases is attributed to the fusion of a portion of the minerals in the mix.

For the mineral phase, an increase in the quantity of albite can be seen from 850 °C to 900 °C. This increase is due to the transformation of nepheline, according to Eqs. (5) and (8). However, the amount of albite also decreases from 950 °C due to the creation of amorphous phases. The same decrease in concentration is observed for all the phases in LCLL Ash, apart for corundum, which shows an increase in concentration of about 3%. Similar results were obtained by Wang et al. (2017) and Chen et al. (2016) for a mixture containing 10% Na_2O.

3.2. Mortar

Compressive strength and relative strength results for mortar samples are respectively presented in Figs. 3 and 4. The relative compressive strength (RCS) of each mortar mix was calculated with the following equation:

$$RCS = \frac{R^{i\ days}_{100\ Cement} - R^{i\ days}_{20SCM}}{R^{i\ days}_{100\ cement}} \quad (10)$$

where the compressive strength of the Portland cement reference and of blended cement with 20% of tested materials at i-days are respectively $R^{i\ days}_{100\ Cement}$ and $R^{i\ days}_{20SCM}$

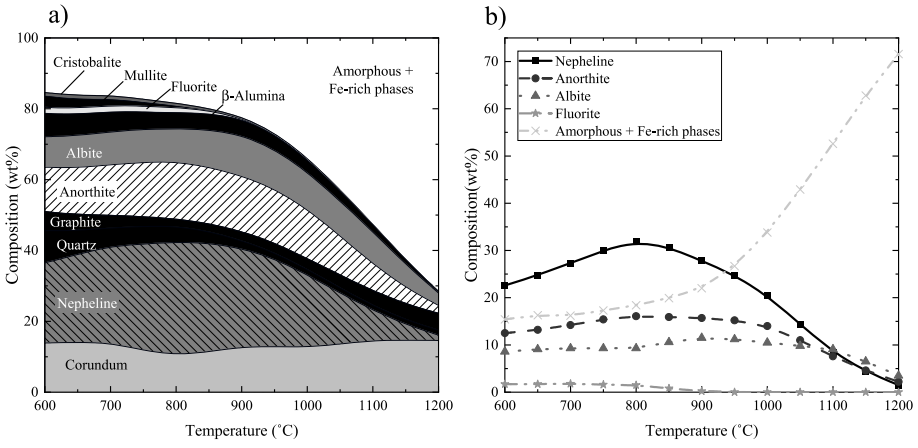

Fig. 2. XRD quantitative analysis of calcined LCLL Ash after cooling.

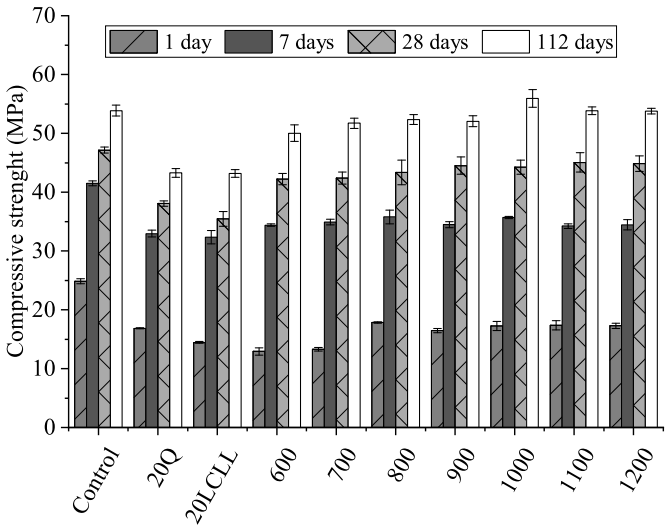

Fig. 3. Compressive strength of mortar with 20% of calcined LCLL Ash replacement at 1, 7, 28, and 112 days (mean values and standard deviation bars).

A decrease of 30%–20% in compressive strength is respectively observed on the mortar samples containing 20% of quartz, at 1 and 112 days. This reduction can be explained by a dilution effect as observed with an increase from 0.485 to 0.610 of the water/binder ratio (Li et al., 2018; Cyr et al., 2005). If a reactive material is incorporated into blended cements, there is an increase in relative strengths to levels higher than quartz due to the hydration of reactive phases which precipitate more hydrates.

According to Fig. 3, LCLL Ash calcined at 600 °C and 700 °C exhibits a lower compressive strength than Portland cement and quartz mortars, with no improvement at 1 and 7 days as compared to LCLL Ash. Therefore, at 28 and 112 days, the compressive strength of LCLL Ash calcined at 600 °C and 700 °C increased to reach a value significantly higher than that of quartz, but lower than that of Portland cement. For LCLL Ash calcined from 800 °C to 1200 °C, the compressive strength results at 1 and 7 days are similar or closer to those of the quartz reference mix. However, these mixes showed values higher than those of quartz and close to those of PC mortar at 28 and 112 days.

As shown in Fig. 4, the tested mortars containing quartz powder showed a reduction around 20%–30% in compressive strength on all the testing days, due to the dilution effect already observed by others (Li et al., 2018; Donatello et al., 2010; Tironi et al., 2013). The relative strength at 1 day of LCLL Ash is lower than the value for quartz by 12%. An even greater delay in gain of compressive strength is observed for LCLL Ash calcined at 600 °C and 700 °C. More than 20% reduction in compressive strength is observed compared to quartz. Calcination at this temperature seems to have increased the delay of LCLL Ash at 1 day. The causes of this delay are not well understood, but they could stem from the presence of graphite in LCLL Ash, as has already been reported for cement (Dutta et al., 1995) and fly ash (Wesche, 1991) hydration, or by the high free alkali concentration (Hewlett and Liska, 2019).

For the mixture calcined at 800 °C, a slightly higher relative strength of 5% was observed. On the other hand, higher calcination temperatures gave results similar to those obtained with quartz, but superior to non-calcined LCLL Ash, which confirms the absence of reactivity and delays for these mixtures. At 7 days, the mixture of non-calcined LCLL Ash somewhat approximates the quartz results, with a reduction of about 20% in compressive strength. For all the other mixtures, we observed values slightly higher to the quartz reference by a little less than 5%. At 28 days, all the calcined mixtures showed relative strengths that were clearly superior to non-calcined LCLL Ash and to the quartz reference, which indicates the presence of reactive phases in the calcined LCLL Ash. Mixtures calcined at 900 °C–1200 °C show greater reactivity with less significant reductions, around 5% and 10% for mixtures calcined at 600 °C and 700 °C. At 112 days, LCLL Ash calcined at 1000 °C–1200 °C shows comparable or better results than Portland cement. Mixtures calcined from 700 °C to 900 °C showed a 5% slight reduction as compared to Portland cement. On the other hand, the mixture calcined at 600 °C showed a reduction of around 7.5%. These results confirm the inert behavior of LCLL Ash and the pozzolanic behavior of calcined LCLL Ash previously observed by (Brial et al., 2021). Considering these results, with a calcination of 2 h, the minimum temperature required to improve LCLL Ash reactivity is 1000 °C.

3.3. Frattini tests

Fig. 5a and b shows, respectively, the calcium concentration as a function of the HO- ion concentration and the calcium reduction measured for LCLL Ash calcined at different temperatures. As for the control containing 100% Portland cement, the non-calcined LCLL Ash and the LCLL Ash calcined at 600 °C are at the same level in the calcium

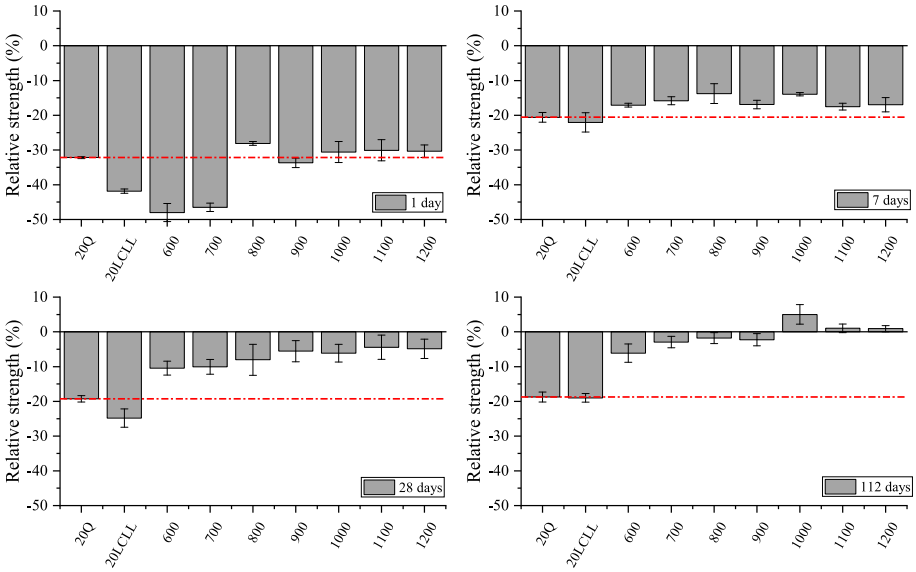

Fig. 4. Relative compressive strength of mortar samples with calcined LCLL Ash at 1, 7, 28 and 112 days. The red line refers to the quartz reference mortar sample.

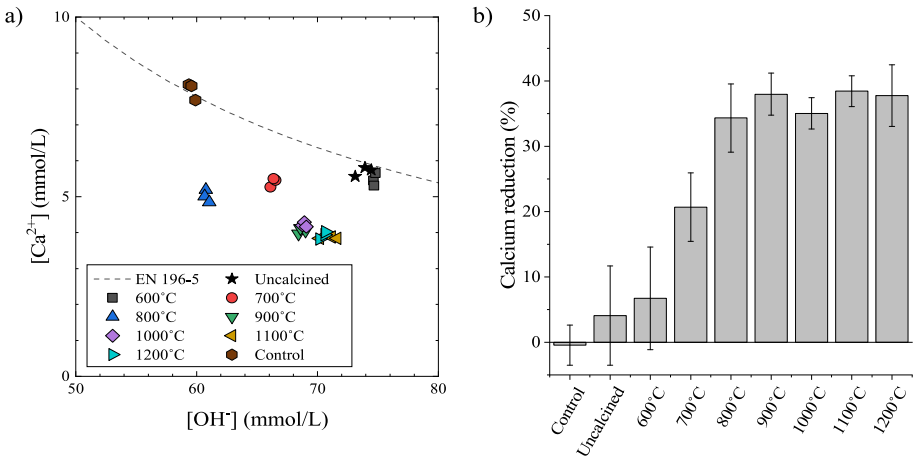

Fig. 5. a) Frattini results for the different calcination temperatures tested. The dashed line refers to the max CaO content according to the EN-196-5 European standard and b) calcium reduction from Frattini test for each calcination temperature tested.

saturation curve given by the European standard. This indicates an absence of pozzolanic reactivity. On the other hand, for calcination temperatures ranging from 700 °C to 900 °C, an increase in reactivity vs. control is observed until a plateau is reached around the 40% reduction level in calcium for higher calcination temperatures. This observation confirms the pozzolanic reactivity of calcined LCLL Ash starting at 700 °C. Comparable results were observed for the non-calcined and calcined mixture at 1050 °C by Brial et al. (2021). In addition, variations are observed in the concentration of HO- ions as a function of the calcination temperature. From 600 °C to 800 °C, a decrease in the concentration of HO- ions is observed, but the concentration increases with an increase of the calcination temperature.

The composition of the solution was also analyzed by ICP to determine the concentrations of K, Na, Al, and Si. The results of the ion concentration analysis are presented in Fig. 6. The potassium concentration for the different calcination temperatures remains similar. However, it is noted that the addition of LCLL Ash increases the concentration of sodium ions by more than 2-fold. However, the sodium concentration decreases at 800 °C and increases again at higher calcination temperatures. This observation explains the variation in pH of the solution as a function of temperature. For Si and Al, an increase in concentration with the calcination temperature is observed, which confirms the better solubility and the increase in reactivity of the calcined LCLL Ash as a function of the calcination temperature.

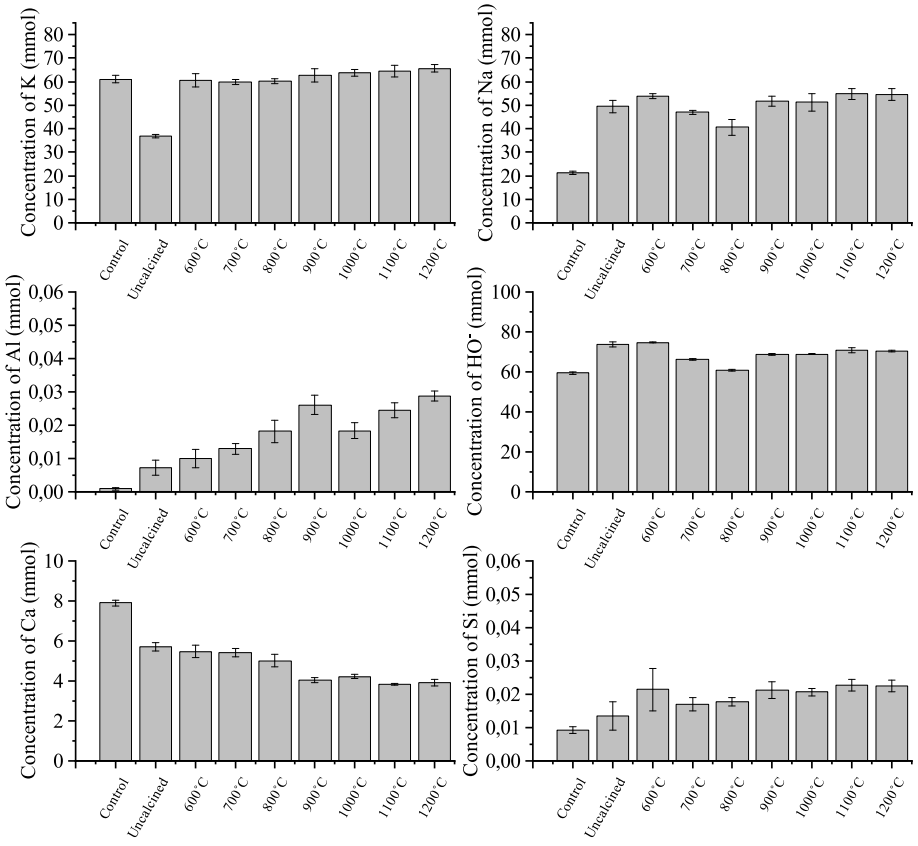

Fig. 6. Concentration in the Frattini solution measured by ICP-OES.

3.4. R^3: heat release and calcium hydroxide consumption

The cumulative heat released and lime consumption obtained after placing the R^3 paste 7 days at 40 °C are respectively shown in Fig. 7a and b. After 7 days, the quartz powder reference showed a weak release of heat of around 25 J/g of SCM, with the portlandite consumption being slightly greater than 30 g/100 g of SCM. The consumption of portlandite by quartz has already been observed in the literature, and is due to a higher pH in the R^3 paste solution and the greater solubility of quartz at 40 °C (Li et al., 2018; Suraneni et al., 2019). However, the low heat released confirms the inert behavior of quartz in the R^3 system. Non-calcined LCLL Ash and LCLL Ash calcined at 600 °C show similar heat outputs, with 210 J/g SCM. A similar result was also obtained for the consumption of portlandite, with results around 62 g/100 g of SCM. Unlike the Frattini results, these two mixtures do not show an inert behavior in the R^3 test. However, as in Brial et al. (2021), the presence of hydroreactivity was observed for these mixtures. In fact, under the conditions of the R^3 test, with a temperature of 40 °C and a higher pH, the hydroreactivity causes the generation of gas and heat in the paste.

At 700 °C, the heat released begins to decrease around 180 J/g of SCM, reaching a minimum value for LCLL Ash calcined at 800 °C with 170 J/g of SCM. For portlandite consumption, the same trend is observed for calcination temperatures from 600 °C to 800 °C, where portlandite consumption levels similar to those of non-calcined LCLL Ash are seen. In addition, the expansion of the paste is still present at 600 °C and 700 °C, but no trace of expansion is visible at 800 °C. For temperatures above 800 °C, the heat released increases as the calcination temperature increases, with values of 210, 230, 250, and 275 J/g of SCM for the calcination temperatures of 900, 1000, 1100, and 1200 °C, respectively. The same trend is observed for the consumption of portlandite going from around 70 g/100 g of SCM at 900 °C to more than 80 g/100 g of SCM for the mixture calcined at 1200 °C. This shows a greater reactivity at these calcination temperatures, similar to the observations made during the Frattini and mortar tests.

Fig. 8 presents the portlandite consumption versus the heat release after 7 days. As shown already by Suraneni et al. (2019), such a relationship can support the classification of the materials tested in function to their types of reactivity: pozzolanic, strongly pozzolanic, hydraulic, and inert. For the quartz powder reference, an inert behavior is clearly identifiable by a low quantity of heat released and a low consumption of portlandite.

In the case of LCLL Ash, calcination behaviors at 600 °C and 700 °C are comparable to those of non-calcined LCLL Ash. However, the presence of hydroreactivity cannot support a pozzolanic behavior in these samples as Eqs. (1)–(3) are exothermic and leads to release aluminum ions in the solution allowing the precipitation of new phases. From

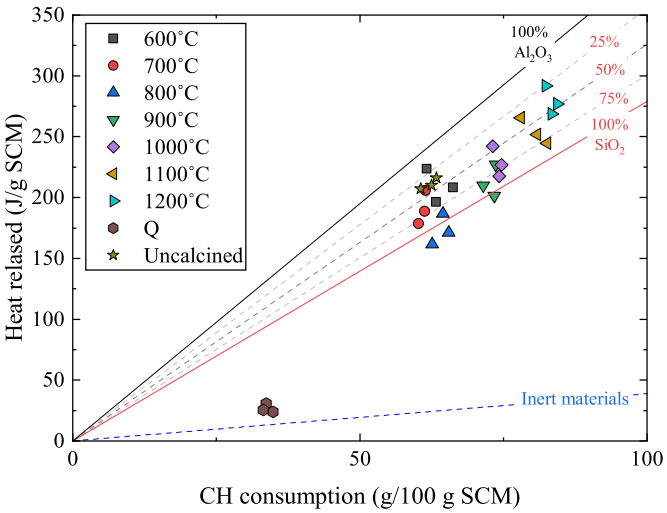

Fig. 8. R^3 test heat released as a function of portlandite consumption for the calcination temperatures studied.

800 °C, the calcination temperature increase tends to increase the pozzolanicity, with a large quantity of heat released and a greater consumption of portlandite.

Thermodynamic simulations on an R^3 system by Brial et al. (2021) were plotted for CaO–SiO_2–KOH (red line), CaO–Al_2O_3–KOH (black line) and CaO–KOH (blue dotted lines) systems. The lines in Fig. 8 show the linear relationship between the portlandite consumption and the heat release of a simulated pozzolanic sample composed only of reactive silica, reactive alumina, and of an inert material respectively represented by the red line, the grey line and the blue dotted line. From these curves, it is possible to predict the ratios of reactive silica/alumina in the pozzolanic materials tested (Brial et al., 2021). For non-calcined and calcined LCLL Ash at 600 °C, a reactive SiO_2/Al_2O_3 ratio of 50%/50% is observed. This ratio is similar to the oxide composition of LCLL Ash. From 600 °C to 800 °C, this ratio drops from around 60%/40% at 700 °C to around 100%/0% at 800 °C. This decrease can be attributed to the decrease in hydroreactivity that occurs. Beyond 800 °C, the reactive SiO_2/Al_2O_3 ratio increases again with the calcination temperature to reach a ratio similar to that of the LCLL Ash, which seems to indicate an optimized reactivity of the calcined LCLL Ash.

3.5. R^3: X-ray diffraction

Fig. 9 presents the XRD data obtained for the R^3 samples extracted

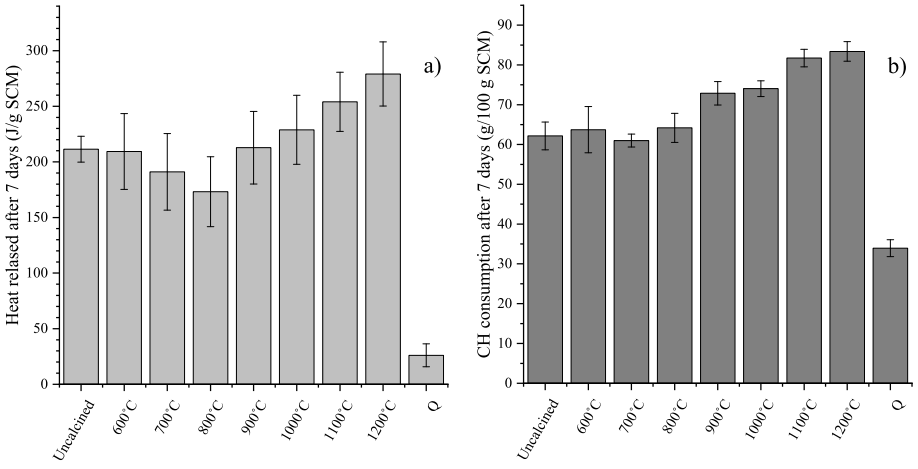

Fig. 7. (a) Heat release and (b) calcium hydroxide consumption after 7 days at 40 °C.

from the calorimetry ampoules. As for portlandite consumption tests, the hydration was stopped by solvent exchange. For the inert quartz powder reference, the major phases were portlandite, calcite and quartz. For non-calcined LCLL Ash, peaks between 10 and 11° 2θ were observed and are respectively associated with monosulfoaluminate (AFm) and hemicarboaluminate (Hc) (Skibsted and Snellings, 2019; Lothenbach et al., 2007; Hewlett et al., 2004). Since LCLL Ash is the only material composed of alumina in the R^3 paste, we can assume that LCLL Ash released in solution of the paste alumina ions, probably due to hydro-reactivity as already reported by Brial et al. (2021). At 600 °C, the same AFm and Hc peaks are visible for calcined and non-calcined LCLL Ash. A new peak at 11.7° 2θ is also observed for the LCLL Ash calcined at 600 °C, showing the precipitation of monocarboaluminate (Mc). At 700 °C, the peaks of monosulfoaluminate (AFm) and hemicarboaluminate (Hc) phases decrease, but the intensity of the monocarboaluminate (Mc) peak is stronger, indicating its higher concentration. A new low intensity peak is also visible around 9° 2θ, which shows the formation of ettringite (AFt). At 800 °C, an increase in AFt and Mc peaks continues to be observed, indicating a higher precipitation of these phases. However, no evidence of AFm and Hc are visible. For higher calcination temperatures, from 900 °C to 1200 °C, the AFt peak disappears and only a strong Mc peak is observed. The intensity of the Mc peak also increases as the calcination temperature increases. Similar results were observed for non-calcined LCLL Ash and LCLL Ash calcined at 1050 °C by Brial et al. (2021).

Fig. 10 shows the crystalline compositions of each R^3 mix were analyzed by Rietveld quantitative analysis. For the quartz powder reference, the formation of amorphous phases and a low consumption of portlandite were observed. This may be related to the lower solubility of quartz, and hence the decreased likelihood of precipitating C–S–H in R^3 experimental conditions. For non-calcined LCLL Ash, indicators of a plausible LCLL Ash reactivity were observed. The portlandite consumption and the precipitation of phases are indicators of possible LCLL Ash reactivity. Additionally, the presence of hemicarboaluminate or monosulfoaluminate confirms the hydro reactive character of LCLL Ash in the R^3 paste as the release of ions containing alumina is associated with reactive compounds (Øye, 2017; Kimmerle et al., 1993). However, LCLL Ash is composed of many crystalline phases that are hardly

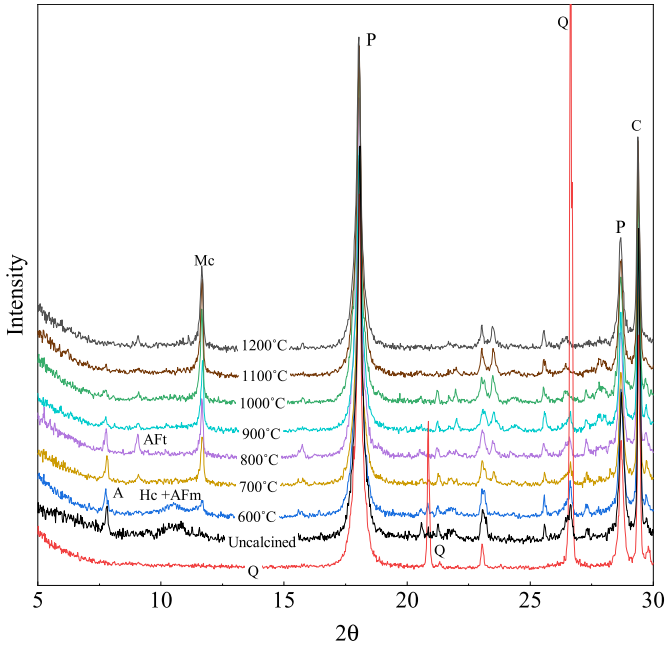

Fig. 9. XRD spectra on R^3 mixes after solvent exchange hydration stoppage (P: Porlandite, Q: Quartz, AFt: Ettringite, Mc: Monocarboaluminate, Hc: Hemicarboaluminate; A: Na-β Alumina).

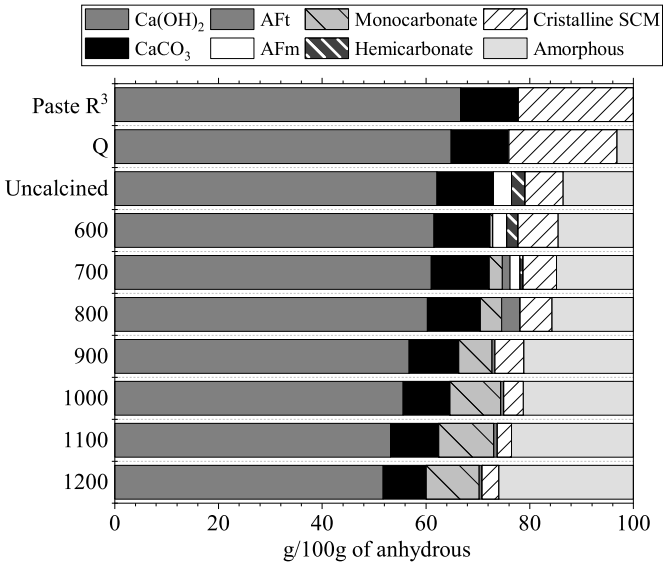

Fig. 10. R^3 mix compositions from quantitative PXRD results after solvent exchange hydration stoppage.

detectable by Rietveld analysis as they are heavily diluted in the R^3 paste. Therefore, they are erroneously perceived as amorphous which limits the likelihood of detecting new amorphous phases associated with reactivity, like C–S–H. This confirms the inert behavior of non-calcined LCLL Ash due to the high concentration of low-soluble phases such as nepheline.

For LCLL Ash calcined at 600 °C, results similar to those obtained with non-calcined LCLL Ash were seen. At 700 °C, new phases start to precipitate, with 1.5 g/100 g of ettringite and 2.5 g/100 g of monocarboaluminate. However, the amorphous content and the portlandite content remain similar to those of uncalcined LCLL Ash. At 800 °C, only ettringite and monocarboaluminate precipitate, and their concentrations increase to 3.5 g/100 g and 4.1 g/100 g of anhydrous, respectively. For higher calcination temperatures (900 °C–1200 °C), the monocarboaluminate concentration increases from 6.5 g/100 g of anhydrous to 10.3 g/100 g of anhydrous indicating a higher solubility of aluminum containing phases. Moreover, the amorphous content also increases from 21 g/100 g–26 g/100 g of anhydrous. In addition, the decreased of portlandite proportion indicates the precipitation of new phases like C–S–H (Scrivener et al., 2016).

4. Discussion

During LCLL Ash calcination, the chemical transformations occurring are similar to reactions seen at high temperatures in coal gasifiers (Li et al., 2012; Wu et al., 2009) and during refractory corrosion in electrolytic tanks (Luneng et al., 2019). The chemical behavior of LCLL Ash at high temperature can be described according to three main phases, namely, nepheline, albite and anorthite. While at an individual level, these phases have very high melting point temperatures, the presence of a eutectic between them can lower the melting temperature of the mix (Lambotte and Chartrand, 2013; Utlak and Besmann, 2018). The phase diagram (Fig. 11a) illustrates the presence of a eutectic for the Albite/Nepheline system. If we consider that all of LCLL Ash's sodium is found in the slag, the $SiO_2/NaAlO_2$ molar ratio of the LCLL Ash is located at the level of the eutectic point, which may explain the creation of amorphous phases at lower temperatures, as the melting temperature of the mix is located at approximately 1080 °C. However, phases such as albite persist even at 1200 °C, which would not seem possible just by looking at the diagram, but because the calcined LCLL Ash has been cooled by air quenching, certain phases, such as albite or nepheline, can be recrystallized. Water quenching could probably have produced a

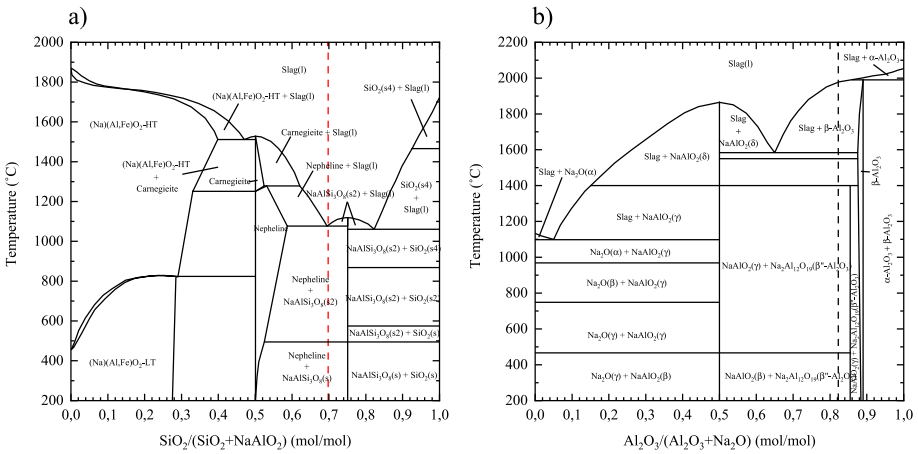

Fig. 11. *$SiO_2/NaAlO_2$ phase diagrams in FACT Database* (Bale et al., 2016). *The red dotted line represents the LCLL Ash molar ratio if all the sodium is present under $NaAlO_2$ and the black dotted line represents the molar ratio Al_2O_3/Na_2O in LCLL Ash.* (For interpretation of the references to colour in this figure legend, the reader is referred to the Web version of this article.)

greater quantity of amorphous due to an increased cooling rate in that context (Wang et al., 2017). The presence of a large amount of sodium is therefore an advantage for calcination since it facilitates the creation of amorphous phases at lower temperatures (Wang et al., 2017; Chen et al., 2016). This allows keeping the calcination temperatures of LCLL Ash lower than that of cement, which places it at a competitive advantage in terms of greenhouse gas emissions.

Calcination leads to a change in the mineralogy of LCLL Ash, allowing the identification of three main types of behavior. From 600 °C to 700 °C, calcined LCLL Ash retains a composition similar to its non-calcined counterpart. Therefore, according to all the observations made, since the mineralogy is similar in both cases, the reactivity behavior is similar to that of non-calcined LCLL Ash in the cement. After calcination at 600 °C, Frattini's test shows a calcium reduction similar to non-calcined LCLL Ash. This calcium reduction slightly increased with calcination at 700 °C. Similar results are observed for the tests of mortar or on the R^3 tests. However, the delay effect at 1 day observed on mortars for non-calcined LCLL Ash (Brial et al., 2021) is greater on mixtures calcined at 600 °C and 700 °C. One of the hypotheses explaining this delay would be the high concentration of rapidly soluble alkalis present in the LCLL Ash which perturb the hydration of C_3A, as shown by (Odler and Wonnemann, 1983; Grzeszczyk and Kucharska, 1990). Despite having similar alkali concentrations between LCLL Ash calcined at 600, 700 °C and at a range of 900 °C–1200 °C according to Frattini solutions results, no retarding effect was seen in mixes calcined at a range of 900 °C–1200 °C. In addition, the mixtures calcined at 600 °C and 700 °C also showed hydroreactivity during the R^3 test. This indicates that calcining at temperatures below 800 °C modifies the solubility of the alkalis, making them more quickly available in the water of the mixture. As shown in Fig. 11b, one hypothesis explaining this would be the transformation of β-alumina into more thermodynamically stable $NaAlO_2$ having a molar ratio of 72% of A_2lO_3 and being more rapidly soluble in water.

At 800 °C, an increase in the proportion of nepheline allows capturing Na_2O in a less soluble phase, which stabilizes a portion of the alkalis. This results in a decreased pH and alkali concentration in the solution. Further, it seems to slightly speed up the setting of compressive strength at 1 day. From a chemical perspective, the hydroreactivity is no longer visible on the R^3 samples. This also presents phases, such as ettringite, not observed on mixtures with higher alkali concentrations. The presence of ettringite is due to the lower concentration of sodium in the solution, as observed by Clark and Brown (2000).

Beyond 800 °C, the proportion of the different phases decreases significantly to form more amorphous phases. This trend can be explained by using a binary SiO_2/Na_2O diagram, where the presence of slag occurs around 850 °C (Lambotte and Chartrand, 2013; Utlak and Besmann, 2018). However, the strong decrease in the quantity of nepheline indicates that a portion of the alkalis will end up in the amorphous phases. This will cause an increase in the concentration of soluble alkalis in the porous solution. However, unlike the mixtures calcined at 600 °C and 700 °C, no delay is observed in the compressive strength at 1 day, which confirms the slower release of the alkalis in the solution. Moreover, from 900 °C to 1200 °C, an increase in reactivity is observed with the increase in the calcination temperature. However, a maximum seems to be reached at 1000 °C, particularly for tests on mortars and Frattini tests. This maximum is not observed, though, for the R^3 tests. XRD analysis of R^3 pastes showed that a calcination temperature above 900 °C provokes a preferential precipitation on monocarboaluminate (Mc). This phenomenon is due to the high CO_3/SO_4 ratio in the R^3 pastes and to alkalis released by LCLL Ash in the solution, which increased the pH (Dow and Glasser, 2003; Feng et al., 2016; Palomo, 2012). The R^3 tests were especially developed to study the reactivity of calcined clay in LC3 mix. The high content of CO_3 available in this mix makes calcining LCLL Ash at 900 °C a better option for making the LC3 mixture (Scrivener et al., 2018).

As for calcined clays, calcination enhances the LCLL Ash reactivity at temperatures above or equal to 800 °C. Moreover, industrial processes requiring high calcination temperatures are necessary to adequately calcine LCLL Ash which has major impacts on the energetic, environmental and financial perspective. Decreasing the temperature of calcination used in conventional Portland cement clinker production, and using a certain percentage of calcined LCLL Ash to replace cement, could further reduce the environmental impacts. From the earlier observations, two calcination temperatures can be distinguished. At 800 °C, the reactivity is slightly lower than the Portland cement at 112 days. However, a portion of the alkalis is captured by nepheline during calcination, which decreases the concentration of alkalis in the porous solution. Calcined at 1000 °C, LCLL Ash showed maximum performance with Portland cement. However, the higher concentration in the pore solution alkali ions, like sodium ions, could be problematic for durability due to gel formation with reactive aggregates. In addition, as shown in Fig. 1b, calcining at 1000 °C requires more grinding energy than LCLL Ash calcined at 800 °C. Thus, due to its higher calcining temperature and longer grinding time, LCLL Ash calcined at 1000 °C will use more energy despite its optimal performance at that temperature.

These results open a new way to sustainably use aluminum SPL by the LCL&L process and with an addition calcination. Despite its optimal calcination temperatures at 800 °C or 1000 °C, the production of calcined LCLL Ash can reduce the carbon footprint of concrete due to the lower calcination temperature than Portland cement clinker, and the

absence of calcite decarbonation. The world production of primary aluminum produces approximately 1.6 million tons of SPL. In the event that all available SPL globally is transformed through the LCL&L industrial process, approximately 480,000 tons of LCLL Ash can be produced. However, these quantities remain relatively low compared to the world production of slag or calcined clay (UN Environment et al., 2018). Moreover, the existence of other SPL processing methods further decreases the volume of LCLL Ash generated. Despite having less impact on the global level of green gas emissions, the main problems associated to SPL, impact the local regions that manage the production of primary aluminum. Indeed, because of the dangerous nature of SPL, spaces for indoor storage and complex transport operations are required. Therefore, the great benefits of using LCLL Ash are primarily seen locally, as it limits the landfill of a hazardous material. Additionally, since 100% of the electricity is produced from renewable energies, in regions such as Quebec, no local fly ashes are produced, which requires importation. In this case, even if the production of LCLL Ash remains low at the global level, environmentally friendly opportunities can exist at a local level like Quebec. This industrial by-product is interesting in area with less clay and conventional SCM readily available.

5. Conclusion

The following concluding remarks can be drawn from the results found in this paper:

a) The use of treated SPL by the LCL&L process for the production of cementitious materials creates new collaborative partnerships between the cement and aluminum industries to lower their environmental impact by reusing a local residual material and reducing landfilling.
b) LCLL Ash calcined at temperatures below 800 °C exhibited reactivity lower than cement. However, the hydroreactivity causing expansion due to gas generation can occur with the increase in the alkali's concentration or the hydration temperature of hydration. At the same time, aluminate ions are released in the pore solution by hydroreactivity, precipitating aluminate phases that may seem to slightly increase LCLL Ash's reactivity.
c) Calcination at 800 °C forms more nepheline, which decreases the alkali concentration in the pore solution. From this temperature, no hydroreactivity is observed, and the reactivity is slightly lower than for the reference Portland cement.
d) The calcination of LCLL Ash from 900 °C to 1200 °C improves significantly its reactivity in cement. Moreover, hydroreactivity is not observed with calcined LCLL Ash at these temperatures. A maximum reactivity was reached by calcining at 1000 °C.
e) Replacing a portion of cement by calcined LCLL Ash could decrease the energetic and environmental impacts of blended cement to produce a more sustainable binder. Treating this hazardous material allows considering LCLL Ash as an alternative to decrease the calcination temperature of cement, provide new ways of valorization, and favors circular economy.
f) Synergies between the primary aluminum and cement production must be further investigated.

Declaration of competing interest

The authors declare that they have no known competing financial interests or personal relationships that could have appeared to influence the work reported in this paper.

Acknowledgments

The authors are grateful to the NSERC Collaborative Research and Development grant program (CRDPJ 515485–17), CRITM consortium, Rio Tinto and Ciment Québec Inc. for their financial support for this project.

References

Agrawal, A., Sahu, K.K., Pandey, B.D., 2004. Solid waste management in non-ferrous industries in India. Resour. Conserv. Recycl. 42, 99–120. https://doi.org/10.1016/j.resconrec.2003.10.004.

Al Jawi, M., Chow, C.M., Pujari, S., Pan, M., Kulkarni, T., Mahmoud, M., Akasha, H., Abdulla, S., 2020. Environmental Benefits of Using Spent Pot Lining (SPL) in Cement Production. Springer International Publishing. https://doi.org/10.1007/978-3-030-36408-3_172.

Ambroise, J., Murat, M., Péra, J., 1985. Hydration reaction and hardening of calcined clays and related minerals V. Extension of the research and general conclusions. Cement Concr. Res. 15, 261–268. https://doi.org/10.1016/0008-8846(85)90037-7.

ASTM International, 2015. C305 − 14 Standard Practice for Mechanical Mixing of Hydraulic Cement Pastes and Mortars. ASTM Stand. B., pp 14–16. https://doi.org/10.1520/C0305-14.2

ASTM International, 2016. C109/C109M − 16a Standard Test Method for Compressive Strength of Hydraulic Cement Mortars Using 2-in . Or [50-mm] Cube Specimens). ASTM Stand. B., pp 1–9. https://doi.org/10.1520/C0109

Bale, C.W., Bélisle, E., Chartrand, P., Decterov, S.A., Eriksson, G., Gheribi, A.E., Hack, K., Jung, I.H., Kang, Y.B., Melançon, J., Pelton, A.D., Petersen, S., Robelin, C., Sangster, J., Spencer, P., Van Ende, M.A., 2016. FactSage thermochemical software and databases, 2010-2016, Calphad Comput. Coupling Phase Diagrams Thermochem. 54, 35–53. https://doi.org/10.1016/j.calphad.2016.05.002.

Birry, B.L., Leclerc, S., 2016. The LCL & L Process, pp. 2–4.

Birry, L., Leclerc, S., Poirier, S., 2016. The Lcl & L Process : a Sustainable Solution for the Treatment and Recycling of Spent Potlining, pp. 467–472.

Brial, V., Tran, H., Sorelli, L., Conciatori, D., Ouellet-Plamondon, C.M., 2021. Evaluation of the reactivity of treated spent pot lining from primary aluminum production as cementitious materials. Resour. Conserv. Recycl. 170, 105584 https://doi.org/10.1016/j.resconrec.2021.105584.

British Standard Euronorm, EN196: Methods of Testing Cement. Part 5: Pozzolanicity Test for Pozzolanic Cement, 2005.

Broek, S., Øye, H.A., 2018. Fundamentals of managing spent potlining (SPL), Trav. 46. In: Proc. 35th Int. ICSOBA Conf, pp. 817–834.

Chen, X.D., Kong, L.X., Bai, J., Bai, Z.Q., Li, W., 2016. Effect of Na2O on mineral transformation of coal ash under high temperature gasification condition. Ranliao Huaxue Xuebao/J. Fuel Chem. Technol. 44, 263–272. https://doi.org/10.1016/s1872-5813(16)30015-9.

Clark, B.A., Brown, P.W., 2000. Formation of calcium sulfoaluminate hydrate compounds. Part II. Cement Concr. Res. 30, 233–240. https://doi.org/10.1016/S0008-8846(99)00234-3.

Cyr, M., Lawrence, P., Ringot, E., 2005. Mineral admixtures in mortars Quantification of the physical effects of inert materials on short-term hydration. Cement Concr. Res. 35, 719–730. https://doi.org/10.1016/j.cemconres.2004.05.030.

Donatello, S., Tyrer, M., Cheeseman, C.R., 2010. Comparison of test methods to assess pozzolanic activity. Cem. Concr. Compos. 32, 121–127. https://doi.org/10.1016/j.cemconcomp.2009.10.008.

Dow, C., Glasser, F.P., 2003. Calcium carbonate efflorescence on Portland cement and building materials. Cement Concr. Res. 33, 147–154. https://doi.org/10.1016/S0008-8846(02)00937-7.

Dutta, D.K., Bordoloi, D., Borthakur, P.C., 1995. Hydration of portland cement clinker in the presence of carbonaceous materials. Cement Concr. Res. 25, 1095–1102. https://doi.org/10.1016/0008-8846(95)00104-K.

Fares, G., 2008. Nouveau systeme cimentaire : cas de la Fritte de verre, These de doctorat présenté en Juillet 2008. Université de Sherbrooke. https://doi.org/10.1177/001088048102200214.

Feng, P., Miao, C., Bullard, J.W., 2016. Factors influencing the stability of AFm and AFt in the Ca – Al – S – O – H system at 25 ° C. J. Am. Ceram. Soc. 1041, 1031–1041. https://doi.org/10.1111/jace.13971.

Friedlingstein, P., O'Sullivan, M., Jones, M.W., Andrew, R.M., Hauck, J., Olsen, A., Peters, G.P., Peters, W., Pongratz, J., Sitch, S., Le Quéré, C., Canadell, J.G., Ciais, P., Jackson, R.B., Alin, S., Aragão, L.E.O.C., Arneth, A., Arora, V., Bates, N.R., Becker, M., Benoit-Cattin, A., Bittig, H.C., Bopp, L., Bultan, S., Chandra, N., Chevallier, F., Chini, L.P., Evans, W., Florentie, L., Forster, P.M., Gasser, T., Gehlen, M., Gilfillan, D., Gkritzalis, T., Gregor, L., Gruber, N., Harris, I., Hartung, K., Haverd, V., Houghton, R.A., Ilyina, T., Jain, A.K., Joetzjer, E., Kadono, K., Kato, E., Kitidis, V., Korsbakken, J.I., Landschützer, P., Lefèvre, N., Lenton, A., Lienert, S., Liu, Z., Lombardozzi, D., Marland, G., Metzl, N., Munro, D.R., Nabel, J.E.M.S., Nakaoka, S.-I., Niwa, Y., O'Brien, K., Ono, T., Palmer, P.I., Pierrot, D., Poulter, B., Resplandy, L., Robertson, E., Rödenbeck, C., Schwinger, J., Séférian, R., Skjelvan, I., Smith, A.J.P., Sutton, A.J., Tanhua, T., Tans, P.P., Tian, H., Tilbrook, B., van der Werf, G., Vuichard, N., Walker, A.P., Wanninkhof, R., Watson, A.J., Willis, D., Wiltshire, A.J., Yuan, W., Yue, X., Zaehle, S., 2020. Global carbon budget 2020. Earth Syst. Sci. Data 12, 3269–3340. https://doi.org/10.5194/essd-12-3269-2020.

Gomes, V., Drumond, P.Z., Neto, J.O.P., Lira, A.R., 2005. Co-processing at cement plant of spent potlining from the aluminum industry. Essent. Readings Light Met. Electrode Technol. Alum. Prod. 4, 1057–1063. https://doi.org/10.1002/9781118647745.ch142.

Grzeszczyk, S., Kucharska, L., 1990. Hydrative reactivity of cement and rheological properties of fresh cement pastes. Cement Concr. Res. 20, 165–174. https://doi.org/10.1016/0008-8846(90)90069-A.

Hewlett, P.C., Liska, M., 2019. Lea's Chemistry of Cement and Concrete, fifth ed. Elsevier. https://doi.org/10.1016/C2013-0-19325-7.

Hewlett, P.C., Bensted, J., Blezard, R.G., Brown, B., Capmas, A., Edmeades, R.M., Eglinton, M., Fidjestel, P., Glasser, F.P., Jackson, P., Jlachowski, E.E., Lewis, R., Macphee, D.E., Massazza, F., Micheline, M.-R., Odler, I., Scrivener, K.L., Sims, I., 2004. Lea's chemistry of cement and concrete. https://doi.org/10.1016/B978-075066256-7/50024-2.

Kajaste, R., Hurme, M., 2016. Cement industry greenhouse gas emissions - management options and abatement cost. J. Clean. Prod. 112, 4041–4052. https://doi.org/10.1016/j.jclepro.2015.07.055.

Kimmerle, F.M., Bernier, J.-L., Kasireddy, V.K., Holywell, G., 1993. Chemical Revovery from Spent PotLining. Miner. Met. Mater. Soc. 671–685.

Laldji, S., Tagnit-Hamou, A., 2016. Glass Frit Concrete as an Alternative Cementitious Material, vol. 10. https://www.researchgate.net/publication/268294095%0AGLASS.

Lambotte, G., Chartrand, P., 2013. Thermodynamic modeling of the (Al2O3 + Na 2O), (Al2O3 + Na2O + SiO 2), and (Al2O3 + Na2O + AlF 3 + NaF) systems. J. Chem. Thermodyn. 57, 306–334. https://doi.org/10.1016/j.jct.2012.09.002.

Lehne, J., Preston, F., 2018. Making Concrete Change- Innovation in Low-Carbon Cement and Concrete.

Li, F.H., Huang, J.J., Fang, Y.T., Wang, Y., 2012. Mineral matter transformation of coal ash under gasification atmosphere: a case of Huolinhe lignite. Adv. Mater. Res. 347–353, 3732–3735. https://doi.org/10.4028/www.scientific.net/AMR.347-353.3732.

Li, X., Snellings, R., Antoni, M., Alderete, N.M., Ben Haha, M., Bishnoi, S., Cizer, Ö., Cyr, M., De Weerdt, K., Dhandapani, Y., Duchesne, J., Haufe, J., Hooton, D., Juenger, M., Kamali-Bernard, S., Kramar, S., Marroccoli, M., Joseph, A.M., Parashar, A., Patapy, C., Provis, J.L., Sabio, S., Santhanam, M., Steger, L., Sui, T., Telesca, A., Vollpracht, A., Vargas, F., Walkley, B., Winnefeld, F., Ye, G., Zajac, M., Zhang, S., Scrivener, K.L., 2018. Reactivity tests for supplementary cementitious materials: RILEM TC 267-TRM phase 1. Mater. Struct. 51, 151. https://doi.org/10.1617/s11527-018-1269-x.

Lothenbach, B., Winnefeld, F., Alder, C., Wieland, E., Lunk, P., 2007. Effect of temperature on the pore solution, microstructure and hydration products of Portland cement pastes. Cement Concr. Res. 37, 483–491. https://doi.org/10.1016/j.cemconres.2006.11.016.

Luneng, R., Bertel, S.N., Mikkelsen, J., Ratvik, A.P., Grande, T., 2019. Chemical durability of thermal insulating materials in hall-héroult electrolysis cells. Ceramics 2, 441–459. https://doi.org/10.3390/ceramics2030034.

Mather, B., 1958. The partial replacement of portland cement in concrete, 100 Barr Harbor Drive, PO Box C700, West Conshohocken, PA 19428-2959. In: Cem. Concr. ASTM International. https://doi.org/10.1520/stp39461s, 37-37–38.

Mejdi, M., Wilson, W., Saillio, M., Chaussadent, T., Divet, L., Tagnit-Hamou, A., 2019. Investigating the pozzolanic reaction of post-consumption glass powder and the role of portlandite in the formation of sodium-rich C-S-H. Cem. Concr. Res. 123, 105790 https://doi.org/10.1016/j.cemconres.2019.105790.

Miller, S.A., John, V.M., Pacca, S.A., Horvath, A., 2018. Carbon dioxide reduction potential in the global cement industry by 2050. Cement Concr. Res. 114, 115–124. https://doi.org/10.1016/j.cemconres.2017.08.026.

Murat, M., 1983. Hydration reaction and hardening of calcined clays and related minerals. I. Preliminary investigation on metakaolinite. Cement Concr. Res. 13, 259–266. https://doi.org/10.1016/0008-8846(83)90109-6.

Nova Pb inc, 2004. Présentation du procédés CalSiFrit. http://142.44.245.8/sections/mandats/alcan-brasque/documents/DM1-1.pdf.

Nunez, P., 2020. Sustainable spent pot line management guidance. Miner. Met. Mater. Ser. 1225–1230. https://doi.org/10.1007/978-3-030-36408-3_168.

Odler, I., Wonnemann, R., 1983. Effect of alkalies on portland cement hydration. Cement Concr. Res. 13, 477–482. https://doi.org/10.1016/0008-8846(83)90005-4.

Øye, H.A., 2017. Discussion of industrial spent pot lining treatment. In: Proc. 35th Int. ICSOBA Conf., Hamburg, Germany, pp. 2–5.

Palomo, A., 2012. Alkaline Hydration of Tricalcium Aluminate, 8, pp. 1–8. https://doi.org/10.1111/j.1551-2916.2012.05348.x.

Personnet, P.B., 1999. Treatment and reuse of spent pot lining, an industrial application in a cement Kiln. In: Essent. Readings Light Met. John Wiley & Sons, Inc., Hoboken, NJ, USA, pp. 1049–1056. https://doi.org/10.1002/9781118647745.ch141.

Scrivener, K., Snellings, R., Lothenbach, B., 2016. A practical guide to microstructural analysis of cementitious materials. https://doi.org/10.7693/wl20150205.

Scrivener, K., Martirena, F., Bishnoi, S., Maity, S., 2018. Cement and concrete research calcined clay limestone cements (LC 3). Cement Concr. Res. 114, 49–56. https://doi.org/10.1016/j.cemconres.2017.08.017.

Shanks, W., Dunant, C.F., Drewniok, M.P., Lupton, R.C., Serrenho, A., Allwood, J.M., 2019. How much cement can we do without? Lessons from cement material fl ows in the UK. Resour. Conserv. Recycl. 141, 441–454. https://doi.org/10.1016/j.resconrec.2018.11.002.

Skibsted, J., Snellings, R., 2019. Reactivity of supplementary cementitious materials (SCMs) in cement blends. Cement Concr. Res. 124, 105799 https://doi.org/10.1016/j.cemconres.2019.105799.

Snellings, R., Chwast, J., Cizer, Ö., De Belie, N., Dhandapani, Y., Durdzinski, P., Elsen, J., Haufe, J., Hooton, D., Patapy, C., Santhanam, M., Scrivener, K., Snoeck, D., Steger, L., Tongbo, S., Vollpracht, A., Winnefeld, F., Lothenbach, B., 2018. Report of TC 238-SCM: hydration stoppage methods for phase assemblage studies of blended cements—results of a round robin test. Mater. Struct. Constr. 51 https://doi.org/10.1617/s11527-018-1237-5.

Strazza, C., Del Borghi, A., Gallo, M., Del Borghi, M., 2011. Resource productivity enhancement as means for promoting cleaner production: analysis of co-incineration in cement plants through a life cycle approach. J. Clean. Prod. 19, 1615–1621. https://doi.org/10.1016/j.jclepro.2011.05.014.

Suraneni, P., Hajibabaee, A., Ramanathan, S., Wang, Y., Weiss, J., 2019. New insights from reactivity testing of supplementary cementitious materials. Cem. Concr. Compos. 103, 331–338. https://doi.org/10.1016/j.cemconcomp.2019.05.017.

Tironi, A., Trezza, M.A., Scian, A.N., Irassar, E.F., 2013. Assessment of pozzolanic activity of different calcined clays. Cem. Concr. Compos. 37, 319–327. https://doi.org/10.1016/j.cemconcomp.2013.01.002.

Tokyay, M., 2016. Cement and Concrete Mineral Admixtures. CRC Press. https://doi.org/10.1201/b20093.

UN Environment, Scrivener, K.L., John, V.M., Gartner, E.M., 2018. Eco-efficient cements: potential economically viable solutions for a low-CO2 cement-based materials industry. Cement Concr. Res. 114, 2–26. https://doi.org/10.1016/j.cemconres.2018.03.015.

Utlak, S.A., Besmann, T.M., 2018. Thermodynamic assessment of the pseudoternary Na2O–Al2O3–SiO2 system. J. Am. Ceram. Soc. 101, 928–948. https://doi.org/10.1111/jace.15166.

Van Oss, H.G., Padovani, A.C., 2003. Cement manufacture and the environment, Part II: environmental challenges and opportunities. J. Ind. Ecol. 7, 93–126. https://doi.org/10.1162/108819803766729212.

Wang, Y., Wang, D., Dong, C., Yang, Y., 2017. The behaviour and reactions of sodium containing minerals in ash melting process. J. Energy Inst. 90, 167–173. https://doi.org/10.1016/j.joei.2016.02.007.

WBCSD, IEA, 2009. Cement Technology Roadmap 2009: Carbon Emissions Reductions up to 2050, p. 36, 978-3-940388-47-6.

WBCSD, 2016. The Cement Sustainability Initiative, Cement Industry Energy and CO2 Performance. Getting the Numbers Right, p. 44. www.wbcsdcement.org/publications%0A?.

Wesche, K., 1991. Fly Ash in Concrete : Properties and Performance. E & FN SPON.

Wu, X., Zhang, Z., Piao, G., He, X., Chen, Y., Kobayashi, N., Mori, S., Itaya, Y., 2009. Behavior of mineral matters in Chinese coal ash melting during char-CO 2/H2O gasification reaction. Energy Fuel. 23, 2420–2428. https://doi.org/10.1021/ef801002n.